








Modulation of cell fate by shock wave therapy in ischaemic heart disease

Michael Graber ^{1,2,†}, Can Gollmann-Tepeköylü^{1,†}, Victor Schweiger¹, Jakob Hirsch ¹, Leo Pölzl ^{1,2}, Felix Nägele¹, Daniela Lener³, Hubert Hackl ⁴, Sieghart Sopper ⁵, Elke Kirchmair¹, Sophia Mair¹, Jakob Voelkl⁶, Christina Plattner⁴, Felix Eichin⁴, Zlatko Trajanoski⁴, Anne Krogsdam⁴, Jonas Eder¹, Manuel Fiegl¹, Dominik Hau¹, Ivan Tancevski ⁷, Michael Grimm¹, John P. Cooke^{8,*}, and Johannes Holfeld ^{1,9,*}

¹Department of Cardiac Surgery, Medical University of Innsbruck, Anichstrasse 35, Innsbruck 6020, Austria; ²Division of Clinical and Functional Anatomy, Medical University of Innsbruck, Anichstrasse 35, 6020 Innsbruck, Austria; ³Department of Internal Medicine, Medical University of Innsbruck, Anichstrasse 35, 6020 Innsbruck, Austria; ⁴Institute of Bioinformatics, Medical University of Innsbruck, Anichstrasse 35, 6020 Innsbruck, Austria; ⁵Department of Hematology and Oncology, Medical University of Innsbruck, Anichstrasse 35, 6020 Innsbruck, Austria; ⁶Institute for Physiology and Pathophysiology, Johannes Kepler University Linz, Linz, Austria; ⁷Department of Internal Medicine II, Medical University of Innsbruck, Anichstrasse 35, 6020 Innsbruck, Austria; ⁸Center for Cardiovascular Regeneration, Department of Cardiovascular Sciences, Houston Methodist Research Institute, 6670 Bertner Ave., Mail Stop: R10-South, Houston, TX 77030, USA; and ⁹Department of Cardiovascular Surgery, German Heart Center Munich, School of Medicine and Health, Technical University of Munich, Lazarettstraße 36, 80636 Munich, Germany

Received 6 September 2024; revised 10 December 2024; accepted 6 February 2025; online publish-ahead-of-print 8 April 2025

Handling Editor: Daniel F.J. Ketelhuth

Aims

Cardiac shockwave therapy (SWT) improves left ventricular (LV) function in patients with ischaemic cardiomyopathy. Shockwave therapy activates Toll-like receptor 3 (TLR3), a receptor-inducing chromatin remodelling and nuclear reprogramming of cardiac cells. We hypothesized that mechanical activation of TLR3 facilitates reprogramming of fibroblasts towards endothelial cells restoring myocardial perfusion and function.

Methods and results

Human cardiac fibroblasts were treated by mechanical stimulation via SWT or TLR3 agonist Poly(I:C) in the presence of endothelial induction medium. A lineage tracing experiment was performed in a transgenic mouse model of Fsp1-Cre/LacZ mice after coronary occlusion. Left ventricular function and scarring were assessed. Single-cell sequencing including RNA trajectory analysis was performed. Chromatin remodelling and epigenetic plasticity were evaluated via western blot and Assay for Transposase-Accessible Chromatin sequencing. Mechanical stimulation of human fibroblasts with SWT activated TLR3 signalling and enhanced the expression of endothelial genes in a TLR3-dependent fashion. The induced endothelial cells (ECs) resembled genuine ECs in that they produced endothelial nitric oxide and formed tube-like structures in Matrigel. In a lineage tracing experiment in Fsp1-Cre/LacZ mice, shockwave treatment increased LacZ/CD31-positive cells (indicating transdifferentiation) after coronary occlusion. Furthermore, SWT reduced myocardial scar size and improved LV function. Single-cell RNA-seq and RNA trajectory analyses revealed that SWT induced an endothelial fibroblast cluster and mechanical stimulation induced significant changes in chromatin organization, with chromatin being more accessible after both treatments in 1705 genomic regions.

Conclusion

Shockwave therapy enhances DNA accessibility via TLR3 activation and facilitates the transdifferentiation of fibroblasts towards endothelial cells in ischaemic myocardium.

* Corresponding author. Email: jpcooke@houstonmethodist.org (J.P.C.); Tel: +435 125 048 0800, Fax: +4351250422527, Email: Johannes.holfeld@i-med.ac.at (J.H.)

† The first two authors contributed equally to the study.

© The Author(s) 2025. Published by Oxford University Press on behalf of the European Society of Cardiology.

This is an Open Access article distributed under the terms of the Creative Commons Attribution-NonCommercial License (<https://creativecommons.org/licenses/by-nc/4.0/>), which permits non-commercial re-use, distribution, and reproduction in any medium, provided the original work is properly cited. For commercial re-use, please contact reprints@oup.com for reprints and translation rights for reprints. All other permissions can be obtained through our RightsLink service via the Permissions link on the article page on our site—for further information please contact journals.permissions@oup.com.

Structured Graphical Abstract

Key Question

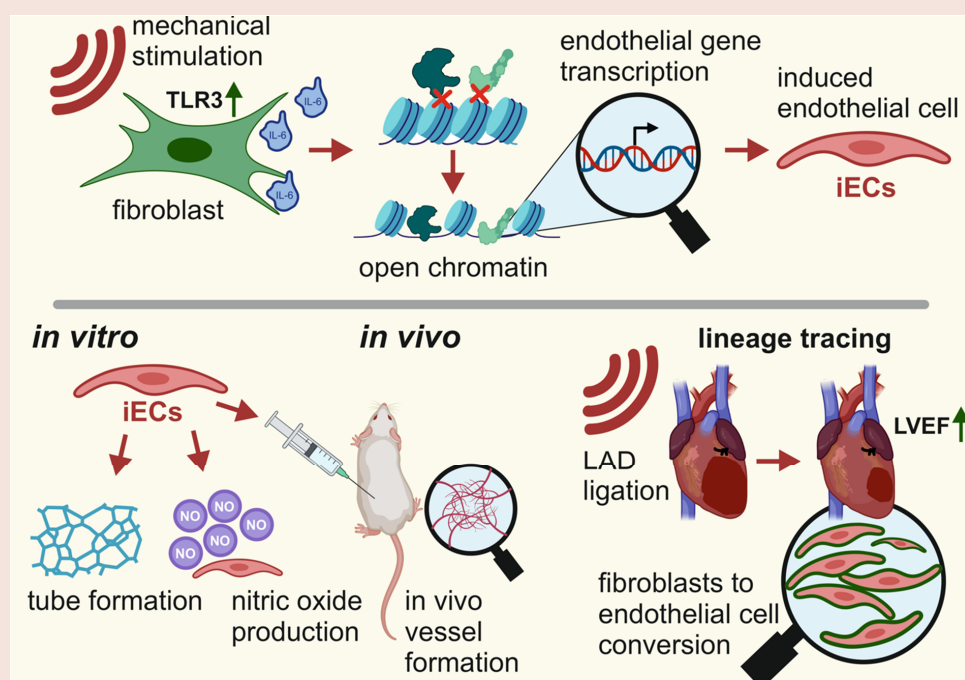
Cardiac shockwave therapy improved LV function in a prospective randomized trial in patients with ischemic cardiomyopathy undergoing coronary bypass surgery. We aimed to elucidate the mechanism underlying the observed regenerative effect of cardiac SWT.

Key finding

SWT activates TLR3 signaling to increase DNA accessibility, facilitating transdifferentiation of cardiac fibroblasts into functional endothelial cells. Therapeutic transdifferentiation increases capillary density, decreased myocardial scarring and hence, improves left ventricular function in ischemic hearts.

Take-home message

We provide evidence for induction of therapeutic transdifferentiation in ischemic myocardium via shockwave therapy. This mechanism be responsible for the beneficial effects of cardiac shockwave therapy observed in the recently published CAST-HF trial.



Keywords

Cardiac surgery • Shockwave therapy • Therapeutic transdifferentiation • Heart regeneration

Translational perspective

The recently published randomized prospective CAST-HF trial showed significant improvement of left ventricular function and exercise capacity after cardiac shockwave therapy in patients with ischaemic cardiomyopathy undergoing coronary bypass surgery. In the current work, we describe the underlying mechanism. Using lineage tracing experiments and transcriptional and epigenetic profiling, we provide evidence that shockwave therapy activates Toll-like receptor 3 signalling to increase DNA accessibility, facilitating therapeutic transdifferentiation of cardiac fibroblasts into endothelial cells.

Summary

Shockwave therapy activates Toll-like receptor 3 signalling to increase DNA accessibility, facilitating transdifferentiation of cardiac fibroblasts into endothelial cells.

Introduction

In the recently published randomized-controlled clinical trial CAST-HF, shockwave therapy (SWT) improved cardiac function, exercise capacity, and quality of life in patients undergoing coronary artery bypass grafting.¹ We discovered that the mechanical impulse is translated into a biological response via the release of angiogenic extracellular vesicles.² Moreover, we could show that the specific activation of TLR3 upon SWT is stimulated by released endogenous RNA.³ Notably, *Tlr3*^{-/-} animals showed no angiogenic response to SWT.

Recently, we and others have considered therapeutic transdifferentiation of fibroblasts to endothelial cells as a potential approach to restoration of perfusion to ischaemic tissues.⁴

This approach derives from the Nobel-prize winning concept that cell fate can be altered by forced expression of lineage determination factors via retroviral induction. Subsequently, other groups used a similar approach to transdifferentiate somatic cells (e.g. fibroblasts) into somatic cells of a different lineage (e.g. endothelial cells) by forced expression of master regulators of the preferred cell lineage.⁵ We have shown that the process of nuclear reprogramming of a somatic cell to another cell fate requires inflammatory signalling. Reprogramming factors themselves are insufficient (as cell-permeant peptides) for effective reprogramming in the absence of the viral vector.⁶ The retroviral vector activates pattern recognition receptors (PRRs) such as Toll-like receptor 3 (TLR3). Activation of PRRs induces inflammatory signalling, which causes global changes in the expression and activity of epigenetic modifiers and their substrates, facilitating the modulation of cell fate.^{7,8} In line with that, we have found that somatic fibroblasts can be transdifferentiated into endothelial cells just by activation of TLR3 and addition of external factors to the cell environment [e.g. endothelial growth factors such as vascular endothelial growth factor (VEGF)].⁷

Accordingly, we hypothesized that SWT induces therapeutic transdifferentiation of cardiac fibroblasts into endothelial cells via activation of TLR3 within the ischaemic heart. The present study tests that hypothesis and provides mechanistic evidence for therapeutic transdifferentiation via SWT.

Methods

Cell culture and induced endothelial cell generation

BJ human newborn foreskin fibroblasts (ATCC, Washington, DC, USA) were cultured and maintained in DMEM with 10% FCS and 1% penicillin/streptomycin/glutamine at 37°C and 5% CO₂. Human umbilical vein endothelial cells (HUVECs) were isolated from umbilical cords of patients undergoing caesarean sections after obtaining written informed consent. The ethics committee of Innsbruck Medical University (No. UN4435) reviewed and approved the study, which also complies to the Declaration of Helsinki. Isolation of HUVECs was performed as described in detail previously.⁹ HUVECs were cultured and maintained in Endothelial Growth Medium 2 (EGM-2, Lonza, Basel, Switzerland) at 37°C and 5% CO₂.

For generation of induced endothelial cells (iECs), BJ fibroblasts were seeded in gelatin-coated flasks and cultured in endothelial induction medium containing DMEM with 10% serum knockout replacement (SKR, Thermo Fisher, Waltham, MA, USA), 20 ng/mL bone morphogenetic protein 4 (BMP4, PeproTech, London, UK), 20 ng/mL basic fibroblast growth factor (bFGF, PeproTech, London, UK), and 50 ng/mL VEGF (PeproTech, London, UK). Cells were treated every other day for 2 weeks with SWT as described previously.¹⁰ Upon last treatment, cell culture media was exchanged to DMEM containing 10% SKR with 20 ng/mL bFGF, 50 ng/mL VEGF, and 0.1 mM 8-bromoadenosine-3':5'-cyclic monophosphate sodium salt (Sigma, St. Louis, MO, USA) until fluorescence-activated cell sorting (FACS) analysis.

Polyinosinic:polycytidylic acid (Poly(I:C); InvivoGen, San Diego, CA, USA) was used to stimulate TLR3 activation at a concentration of 30 ng/mL. This concentration was chosen based on prior dose-ranging studies. For blockade of TLR3, a dsRNA/TLR3 complex inhibitor (R)-2-(3-chloro-6-fluorobenzo[b]thiophene-2-carboxamido)-3-phenyl-propanoic acid was used (Merck, Darmstadt, Germany) at a concentration of 10 µg/mL.⁹

For inhibition experiments, STAT3 inhibitor peptide (Sigma, St. Louis, MO, USA), IL-6 inhibitor LMT28 (Sigma, St. Louis, MO, USA), and IκB kinase inhibitor (ab145522, abcam, Cambridge, UK) were used.

Shockwave therapy

Shockwave therapy has been used for mechanical stimulation in a recent clinical trial (CAST-HF trial, ClinicalTrials.gov, ID: NCT03859466). We used a prototype of the NRG device with the CSP applicator (Heart Regeneration Technologies GmbH, Innsbruck, Austria). For the *in vivo* application, 300 impulses were delivered to the ischaemic area with an energy flux density of 0.38 mJ/mm² at a frequency of 5 Hz.

Fluorescence-activated cell sorting

Upon induction of endothelial transdifferentiation, cells were analysed and purified with FACS. Cells were dissociated with recombinant trypsin (TrypLE, Thermo Fisher, Waltham, MA, USA) and washed with 1% Bovine serum albumin (BSA) in phosphate buffered saline (PBS). Cells were afterwards incubated with a PE-conjugated CD31 antibody (Miltenyi, Bergisch Gladbach, Germany) for 15 min. Gating strategy was defined by positive control staining of HUVECs. Upon cell sorting, cells were re-cultured in EGM-2 supplemented with 10 µM transforming growth factor beta (TGF-β) receptor inhibitor SB431542 (Merck, Darmstadt, Germany) to promote endothelial cell growth.⁷

Immunofluorescence staining

Cells were seeded on gelatin-coated coverslips and fixed with 100% methanol. Upon blocking with 10% normal goat serum in PBS, cells were incubated with anti-CD31 antibody (ab28364, Abcam, Cambridge, UK) for 1 h at a dilution of 1:100. After careful washing with PBS, incubation in the dark with secondary antibody (AlexaFluor568 goat-anti-rabbit) followed. Counterstaining was done with DAPI and coverslips were mounted on the slides.

Tube formation assay

A 96-well plate was coated with Matrigel (Corning, Corning, NY, USA), and cells were seeded at a density of 10⁴ cells/well. Cells were incubated with

EGM-2 for 24 h and phase-contrast images were obtained. Automated quantification of tube formation was assessed by using the angiogenesis analyzer plugin software in NIH ImageJ as described before.¹¹

Nitric oxide production

Nitric oxide (NO) production was assessed by using a NO detection kit (R&D Systems, Minneapolis, MN, USA) according to the manufacturer's instructions. The total amount of NO in supernatant of cells was assessed using the Griess reaction and quantified by colorimetric measurement using a microplate reader.

Matrigel plug assay

The *in vivo* Matrigel angiogenesis assay was performed as described previously.¹² Briefly, Matrigel (Corning, Corning, NY, USA) was mixed with 5×10^5 cells to a total volume of 300 μ L and injected subcutaneously in immunodeficient NOD SCID gamma mice. Upon 5 days, blood perfusion was measured with laser Doppler imaging. Plugs were harvested and fixed in 4% formalin overnight prior to histological processing.

RNA extraction and Reverse transcription polymerase chain reaction

Total RNA was extracted by using a Monarch Total RNA Miniprep Kit (New England Biolabs, Ipswich, MA, USA) according to the manufacturer's instructions. Integrity of RNA was assessed by using a NanoDrop™ 2000c spectrophotometer, and reverse transcription polymerase chain reaction (RT-PCR) was performed with ABI PRISM 7500 Sequence Detection System (Applied Biosystems, Foster City, CA, USA). Specific gene expression was expressed as $2^{-\Delta CT}$ formula by normalizing to the housekeeping gene glyceraldehyde 3-phosphate dehydrogenase (GAPDH). The following primer sequences were used:

IL-6	5' AGCCACTCACCTCTTCAGAAC 3'
	5' AGTGCCCTCTTTGCTGCTTC 3'
CD31	5' ACACGGAAGTTCAGGTGCC 3'
	5' AAGTCCATCAAGGGAGCCTTC 3'
VEGF receptor 2 (VEGFR2)	5' ACCTCACCTGTTTCTCTGTATGG 3'
	5' CGGCTCTTCGCTTACTGTTC 3'
Vascular endothelial cadherin (VE-Cadherin)	5' ACCAGAAGAAGCCTCTGATTGG 3'
	5' AGAACTGGCCCTTGCTCACTG 3'
Histone deacetylase 1 (HDAC1)	5' TATGGACAAGGCCACCCAA TG 3'
	5' TATGGACAAGGCCACCCAATG 3'
GAPDH	5' GGTGGTCTCCTCTGACTTCAACA 3'
	5' GTGGTCGTTGAGGGCAATG 3'

Western blot

Total nuclear and cytoplasmic protein from cell lysates were extracted by a subcellular protein fractionation kit (Thermo Fisher, Waltham, MA, USA) according to the manufacturer's instructions. Protein was separated with 10% SDS-polyacrylamide gels and transferred to nitrocellulose membranes. Upon blocking with 5% BSA in 0.1% Tween/TBS, membranes were incubated with primary antibodies.

The following antibodies were used:

TLR3	Cell Signaling, #6961
TIR-domain-containing adapter-inducing interferon- β (TRIF)	
Cell Signaling, #4596	
TRAF6	Cell Signaling, #8028
IL-6-R	Abcam, ab103798
β -Actin	Sigma, Clone AC-15
pSTAT3	Cell Signaling, #9138
H3K4me3	Abcam, ab8580
PR-domain-containing transcriptional regulator 14 (PRDM14)	
R&D systems, AF6175	
TBP	Cell Signaling, #8515
H3	Abcam, ab1791

After incubation with secondary antibody and chemiluminescence substrate, western blots were visualized using a ChemiDoc Imaging System (Bio-Rad, Hercules, MA, USA).

Toll-like receptor 3 reporter cell assay

A stable transfected human embryonic kidney reporter cell line (Human TLR3 Stable Cell Line NBP2-26267, Novus Biologicals, Centennial, CO, USA) was cultured on gelatin-coated wells in DMEM 4.5 g/L glucose (Lonza, Basel, Switzerland) with 10% FCS and 1% penicillin/streptomycin/glutamine. Shockwave therapy as well as Poly(I:C) administration was performed as described above and cells were incubated for 24 h. Detection of secreted embryonic alkaline phosphatase under the transcriptional control of nuclear factor kappa B (NF- κ B) was assessed by using a colorimetric alkaline phosphatase reporter assay kit (Novus Biologicals, Centennial, CO, USA) according to the manufacturer's protocol.

Single-nucleus RNA sequencing

Nucleus isolation and sequencing

Left ventricles were harvested from 12 male mice (12 weeks). Hearts were rinsed with PBS and left ventricles were snap-frozen in liquid nitrogen. Nuclei were isolated using the 10 \times Chromium nucleus isolation kit (10 \times Genomics, Pleasanton, USA) according to the manufacturer's protocol. In brief, tissue was homogenized using a pestle and lysis buffer. Nuclei were isolated from the disrupted sample and separated from debris using the provided spin columns. >80,000 DAPI-positive nuclei per sample were sorted from the resulting suspension using FACSaria III Cell Sorter (BD Bioscience, Franklin Lakes, NJ, USA). The single-nucleus suspensions were processed with the Chromium Instrument (10 \times Genomics) targeting 10,000 nuclei per sample and using Chromium Next GEM Single Cell 3' Kit v3.1 chemistry, following the manufacturer's protocol (CG000204 Rev D, 10 \times Genomics). The 12 resulting libraries were multiplexed and sequenced with an Illumina NovaSeq sequencer, employing one S4 lane to obtain a total of 2.3 B reads.

Pre-processing and filtering

Sequencing reads from the 12 samples were pre-processed and mapped to the reference mouse genome GRCm39/mm39 using the nf-core/scrnaseq pipeline version 2.1.0¹³ with cellranger as the selected aligner.

The data set was then loaded into an AnnData container, and quality control steps and filtering were performed with scanpy v1.9.1¹⁴ in Python v3.10.8. We applied a basic filtering for nuclei expressing <200 genes and for genes present in less than three nuclei.

Ambient RNA was removed separately for each sample with the scAR implementation¹⁵ from scvi-tools.¹⁶ One sample (SWT14D) was excluded after this step, since it contained mainly ambient RNA, as we have also seen by visual inspection of the quality control plots in the previous step.

For doublet removal, we used the SOLO¹⁷ implementation from scvi-tools.¹⁶ As recommended by the authors, SOLO was initialized with a pre-trained scvi-model. In total, 30 990 doublets were removed from the remaining 11 samples. Final manual filtering of low-quality nuclei was applied for nuclei, expressing a minimum of 500 genes and a maximum of 8200 genes and for nuclei containing a high mitochondrial content (>5% of total unique molecular identifier (UMI)).

Clustering and cell type annotation

Uniform manifold approximation and projections embeddings and unsupervised clustering with the Leiden algorithm were performed based on a cell-cell neighbourhood graph derived from scVI latent space. The final matrix was normalized and log-transformed using the `scanpy.pp.normalize_total()` and `scanpy.pp.log1p()` functions.

Cell types were annotated according to known cell markers (see [Supplementary material online, Figure S2A](#)) from literature^{18–20} and clusters aggregated accordingly.

Subclustering and pseudotemporal ordering of fibroblasts

To evaluate the differences in fibroblasts specifically, the fibroblast cluster was subsetted, and clusters were recalculated the same way as described above. We found 10 different fibroblast clusters with a resolution of 0.5.

For visualizing possible dynamics in the fibroblast clusters, we applied pseudotemporal ordering of the nuclei.²¹ First, diffusion maps were calculated with the *scanpy.tl.diffmap()* function. Then, the root cell was defined as the minimum of the diffusion component 3, and the pseudotimes were constructed with the *scanpy.tl.dpt()* function. Finally, partition-based graph abstraction (PAGA)²² was computed to estimate the connections between the clusters. The PAGA graph was visualized with *scanpy.pl.paga()*, removing low-connectivity edges (threshold: 0.1), and coloured according to the computed dpt-pseudotime.

Analysis of Assay for Transposase-Accessible Chromatin data

For data analysis of the Assay for Transposase-Accessible Chromatin sequencing (ATAC-seq), reads from paired-end sequencing were trimmed for adapters and low-quality bases using Trimmomatic 0.38, aligned to the human reference genome hg38 using bowtie2, and filtered using samtools 1.9 (alignments that have a minimum mapping quality of 30 were aligned concordantly and used as primary alignments). Duplicates were marked using Picard 2.18.26 and removed. Prior to peak calling, reads mapping to mitochondria and unlocalized/unplaced contigs were removed. MACS2 2.1.2 was used for peak calling to identify open chromatin regions. Called peaks in blacklisted regions (hg38) were filtered and overlapping peaks within each sample were merged. Following the csaw R workflow,²³ consensus peak regions were identified by union of significant peaks in each sample using *GenomicRanges* R package. A sliding window approach (*windowCounts*) with 300 bp width was used to count fragments from the alignments (bam files) in these regions. Normalization factors were calculated using trimmed mean of *M*-value on non-overlapping (binned) 10 000 bp windows. Differentially accessible regions between the Poly(I:C) group vs. CTRL group and SWT group vs. CTRL group were determined with the *edgeR* package, filtered for regions with low average log normalized counts > 0, and visualized as volcano plots. *ChIPseeker* and *TxDb.Hsapiens.UCSC.hg38.knownGene* R packages were used to find the nearest genes (transcription start site) and to annotate gene/transcript regions. Heatmap of standardized normalized counts of significantly differentially accessible regions (unadjusted $P < 0.01$ in both comparisons) was visualized using *Genesis* 1.8.1. Over-represented gene ontology terms were identified using DAVID. Coverage tracks (igwig) for UCSC genome browser visualization were generated from paired-end sequencing read alignment (bam files) using R packages *GenomicAlignments* and *rtracklayer*. Merged peaks and differentially accessible regions were transformed from bed to bigbed format using UCSC tools (*bedToBigBed*).

Animals and induction of myocardial infarction

Ethical permission (BMWFW-66.011/0020-WF/V/3b/2017) of animal experiments was obtained and experiments were performed according to the 'Guide for the Care and Use of Laboratory Animals' published by the US National Institutes of Health.²⁴ Experiments were performed in fibroblast specific-targeted mutant mice (FSP1cre; Stock No: 030644) crossed with ROSA26-lacZ reporter mice (Stock No: 002073; both purchased by Jackson Laboratory, Bar Harbor, ME, USA).

Myocardial infarction was performed by ligation of the left anterior descending coronary artery (LAD) in 12- to 15-week-old FSP1cre:R26RlacZ mice. Animals were anaesthetized via intraperitoneal injection of ketamine hydrochloride (80 mg/kg body weight) and xylazine hydrochloride (5 mg/kg body weight). After lateral thoracotomy, the LAD was ligated using 8-0 polypropylene sutures (Ethicon, Somerville, NJ, USA). All surgical procedures were performed in a blinded fashion.

Upon layered wound closure, extracorporeal SWT was performed as described previously.²⁵

Echocardiography

To assess functional parameters of cardiac function, transthoracic echocardiography was performed as described previously.²⁶ In brief, mice were subjected to anaesthesia with isoflurane 1.5% (AbbVie, North Chicago, IL, USA) and 98.5% O₂ and placed on a warming pad at 37.5°C before and during the procedure. Measurements were performed with the Vevo 1100 imaging system and Visual Sonics Software Vevo Lab 1.7.1 (Visual Sonics, Toronto,

Canada) and a MS400 (18–38 MHz) transducer. Systolic function was assessed in parasternal longitudinal axis in B-Mode, and ventricular wall dimensions were assessed on papillary muscle level in M-Mode. All measurements and analyses were performed in a blinded fashion.

Histopathological analysis

Twenty-eight days after myocardial infarction, mice were euthanized and hearts were dissected. Hearts were fixed in 4% paraformaldehyde for 24 h and embedded in paraffin.

Sections were stained with Masson–Goldner trichrome stain as described previously.²⁷ Quantification of fibrotic area was assessed by using the NIH ImageJ software.

For immunofluorescence staining, sections underwent a heat-mediated antigen retrieval in sodium-citrate buffer (10 mM sodium-citrate, 0.05% Tween 20, pH 6.0). Upon washing with PBS and blocking, slides were incubated with primary antibodies anti-CD31 (ab28364, Abcam, Cambridge, UK) and anti-β-galactosidase (ab9361, Abcam, Cambridge, UK) overnight. As secondary antibodies, AlexaFluor488 and AlexaFluor568 were used. Counterstaining was performed with DAPI and sections were imaged with a SP8 confocal microscope (Leica, Wetzlar, Germany). The infarct border zone was analysed to assess therapy effects in the area with the most pronounced cellular changes and highest potential for therapeutic impact.

All measurements and analyses were performed in a blinded fashion.

Statistical analysis

Graphs are presented as scatter/dot plots and results are expressed as mean ± SEM. Statistical comparisons between two groups were performed by Student's *t*-test, multiple groups were analysed by one-way analysis of variance (ANOVA) with Tukey *post hoc* analysis to determine statistical significance. *P*-values of <0.05 were considered statistically significant, if not stated otherwise.

Specific statistical data were analysed in figures:

Figure 1B: ordinary one-way ANOVA: $F(2, 15) = 790.0$; $P < 0.0001$; $n = 6$.

Figure 1D: two-tailed *t*-test: $t = 3.842$, $df = 10$; $P = 0.0033$; $n = 6$.

Figure 1F: ordinary one-way ANOVA: $F(3, 20) = 61.19$; $P < 0.0001$; $n = 6$.

Figure 1G: ordinary one-way ANOVA: $F(3, 18) = 9.531$; $P = 0.0005$; $n = 5–6$.

Figure 1H: ordinary one-way ANOVA: $F(3, 20) = 41.42$; $P < 0.0001$; $n = 6$.

Figure 2A: two-tailed *t*-test: $t = 4.469$, $df = 10$; $P = 0.0012$; $n = 6$.

Figure 2B: two-tailed *t*-test: $t = 6.610$, $df = 10$; $P < 0.0001$; $n = 6$.

Figure 2E: two-tailed *t*-test: $t = 9.288$, $df = 16$; $P < 0.0001$; $n = 9$.

Figure 2F: two-tailed *t*-test: $t = 9.092$, $df = 16$; $P < 0.0001$; $n = 9$.

Figure 2G: two-tailed *t*-test: $t = 7.118$, $df = 10$; $P < 0.0001$; $n = 6$.

Figure 2I: ordinary one-way ANOVA: $F(2, 15) = 46.66$; $P < 0.0001$; $n = 6$.

Figure 2L: ordinary one-way ANOVA: $F(2, 14) = 4.476$; $P = 0.0314$; $n = 5–6$.

Figure 3C: two-tailed *t*-test: $t = 2.276$, $df = 8$; $P = 0.0524$; $n = 5$.

Figure 3E: two-tailed *t*-test: $t = 3.730$, $df = 8$; $P = 0.0058$; $n = 5$.

Figure 3F: two-tailed *t*-test: $t = 4.369$, $df = 8$; $P = 0.0024$; $n = 5$.

Figure 3G: two-tailed *t*-test: $t = 1.597$, $df = 8$; $P = 0.1490$; $n = 5$.

Figure 3I: two-tailed *t*-test: $t = 5.271$, $df = 28$; $P < 0.0001$; $n = 4–6$, 3hpf per n.

Results

Shockwave therapy induces transdifferentiation via Toll-like receptor 3

We stained human cardiac fibroblasts for TLR3 and found abundant expression of the innate immune receptor (Figure 1A). Shockwave therapy activated TLR3 signalling in reporter cells, with subsequent up-regulation of the downstream adapter TRIF and transcription of IL-6 (Figure 1B–D). We next assessed whether TLR3 activation upon SWT facilitates the conversion of fibroblasts to iECs in the presence of a specific induction medium known to promote endothelial lineage (i.e. DMEM with 10% SKR containing BMP4, VEGF, and FGF) as described previously⁷ (Figure 1E). Here, the rationale is that the SWT

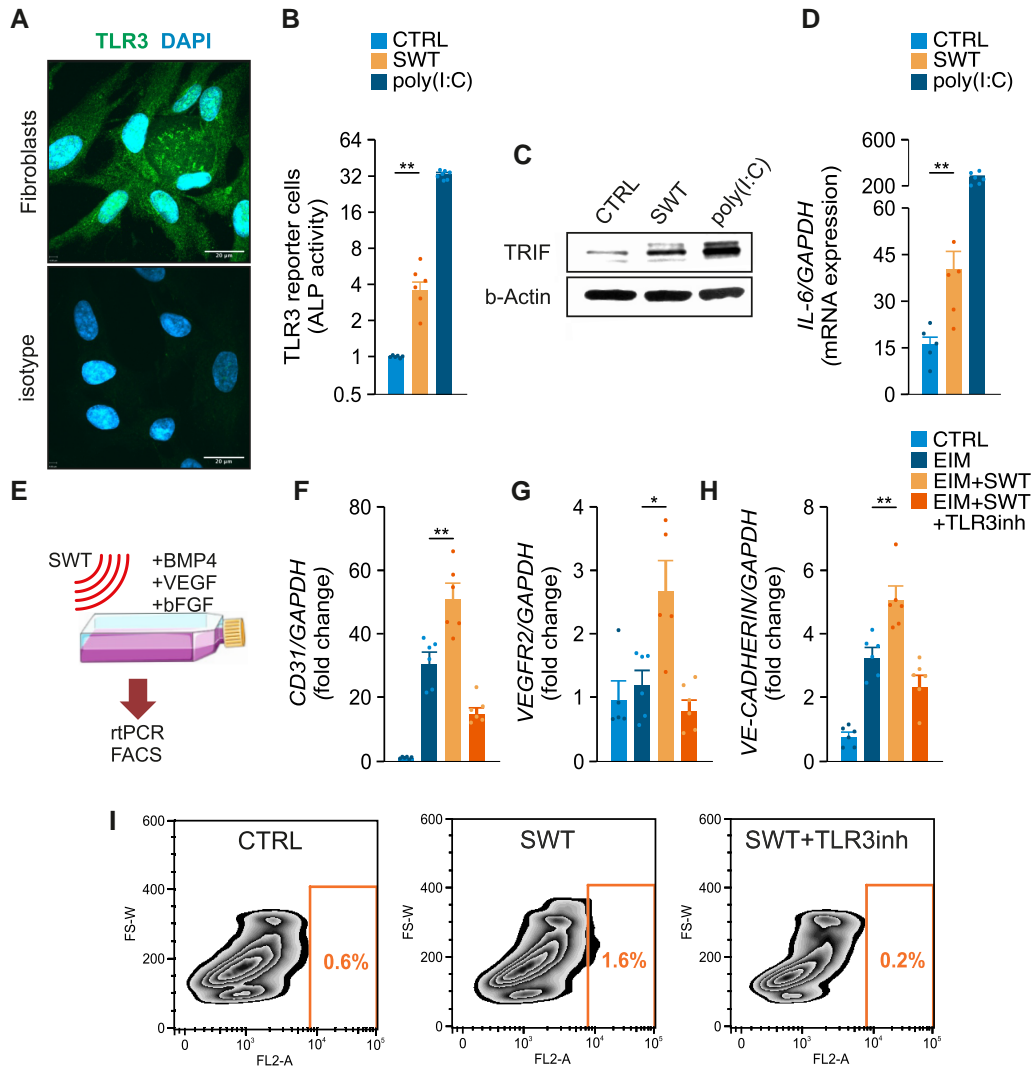


Figure 1 Shockwave therapy induces transdifferentiation via Toll-like receptor 3. (A) Expression of the innate immune receptor Toll-like receptor 3 on human cardiac fibroblasts. green = Toll-like receptor 3; blue = DAPI. Scale bar = 20 μ m. (B) Toll-like receptor 3 activation of Toll-like receptor 3 reporter cells upon shockwave therapy or Poly(I:C) treatment (30 ng/mL). Data are means \pm SEM. $^{**}P < 0.01$. (C) The expression of the downstream adapter TIR-domain-containing adapter-inducing interferon- β after shockwave therapy or Poly(I:C) treatment (30 ng/mL). (D) mRNA levels of interleukin-6 after shockwave therapy or Poly(I:C) treatment (30 ng/mL). Data are means \pm SEM. $^{*}P < 0.01$. (E) Human fibroblasts were treated with shockwave therapy in the presence of endothelial induction medium containing bone morphogenetic protein 4, vascular endothelial growth factor, and fibroblast growth factor and subjected to reverse transcription polymerase chain reaction (RT-PCR) or fluorescence-activated cell sorting. (F) mRNA expression of CD31 after treatment with control medium, endothelial induction medium, shockwave therapy, or a specific dsRNA/Toll-like receptor 3 inhibitor. Data are means \pm SEM. $^{**}P < 0.01$. (G) mRNA expression of VEGF receptor 2 after treatment with control medium, endothelial induction medium, shockwave therapy, or a specific dsRNA/Toll-like receptor 3 inhibitor. Data are means \pm SEM. $^{*}P < 0.05$. (H) mRNA expression of vascular endothelial cadherin after treatment with control medium, endothelial induction medium, shockwave therapy, or a specific dsRNA/Toll-like receptor 3 inhibitor. Data are means \pm SEM. $^{**}P < 0.01$. (I) Fluorescence-activated cell sorting for CD31 after treatment with shockwave therapy or a combined treatment with a specific dsRNA/Toll-like receptor 3 inhibitor and shockwave therapy. Statistical comparisons between multiple groups: one-way analysis of variance with Tukey *post hoc* analysis. ALP, alkaline phosphatase; BMP4, bone morphogenetic protein 4; CTRL, control; EIM, endothelial induction medium; FACS, fluorescence-activated cell sorting; FGF, fibroblast growth factor; GAPDH, glyceraldehyde 3-phosphate dehydrogenase; IL-6, interleukin-6; SWT, shockwave therapy; TLR3, Toll-like receptor 3; TLR3inh, TLR3 inhibitor; TRIF, TIR-domain-containing adapter-inducing interferon- β ; VE-cadherin, vascular endothelial cadherin; VEGF, vascular endothelial growth factor; VEGFR2, VEGF receptor 2.

activates inflammatory signalling to increase DNA accessibility, whereas the induction medium comprises endothelial growth factors that provide transcriptional direction. Indeed, the combination of SWT and induction medium triggered the expression of endothelial genes in

fibroblasts including CD31, VEGFR2, and vascular endothelial cadherin (VE-cadherin) to a markedly higher extent than treatment with induction medium alone (Figure 1F–H). In this context, the addition of a specific dsRNA/TLR3 complex inhibitor abolished the induction of

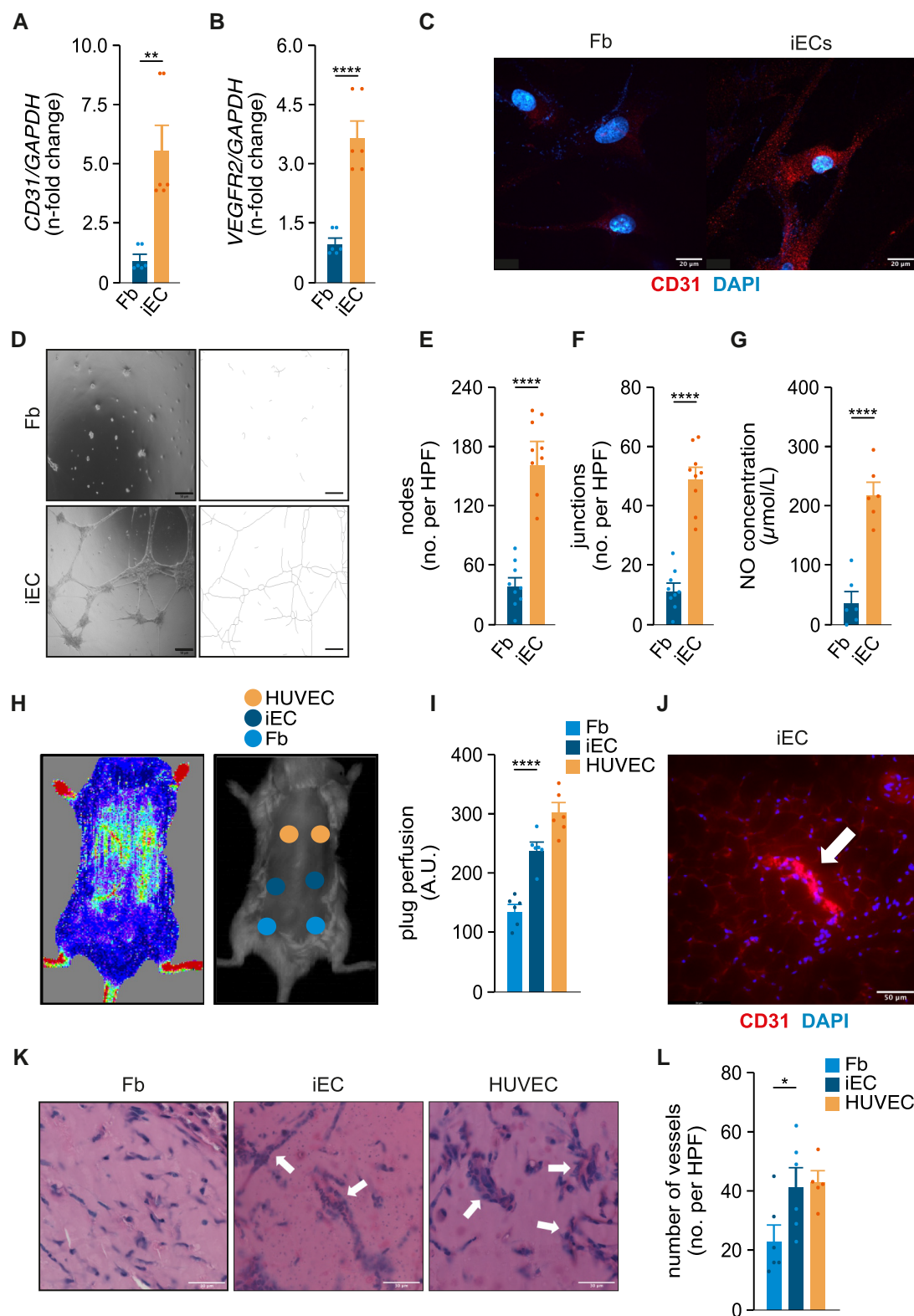


Figure 2 Induced endothelial cells are functional *in vitro* and *in vivo*. (A) mRNA expression of CD31 after fluorescence-activated cell sorting of induced endothelial cells or fibroblasts. Data are means \pm SEM. ** P < 0.01. (B) mRNA expression of vascular endothelial growth factor receptor 2 after fluorescence-activated cell sorting of induced endothelial cells or fibroblasts. Data are means \pm SEM. **** P < 0.0001. (C) CD31 expression of induced (continued)

endothelial gene expression after SWT (Figure 1F–H). To purify the iECs, cells underwent FACS for CD31.

Combined treatment with SWT and induction medium induced CD31 expression in 1.6% of the treated cells, whereas only 0.6% were positive after treatment with induction medium alone. Again, pre-treatment with a TLR3 inhibitor abolished SW effects (Figure 1I). The effect of SWT to enhance transdifferentiation is quantitatively similar to that induced by TLR3 agonists.⁸

Altogether, our results indicate that SWT promotes the transdifferentiation of fibroblasts to endothelial cells in a TLR3-dependent fashion.

Induced endothelial cells are functional *in vitro* and *in vivo*

Sorted iECs continued to express endothelial genes including CD31 and VEGFR2 in culture (Figure 2A and B). Similarly, iECs were positive for CD31 by immunohistochemistry (Figure 2C). The iECs were able to form tube-like structures on Matrigel (Figure 2D–F) and capable of producing NO (Figure 2G), functions that are characteristic of endothelial cells and not shared by fibroblasts.

In a next series of experiments, we assessed SWT-induced ECs for their capability to form vessels *in vivo*. For this purpose, cardiac fibroblasts were transdifferentiated to iECs as described above and sorted thereafter for CD31. Induced endothelial cells were suspended in Matrigel and injected subcutaneously into SCID mice. Untreated HUVECs and fibroblasts were used as positive and negative controls, respectively (Figure 2H). Induced endothelial cell-containing plugs manifested increased perfusion compared with fibroblast-containing plugs measured via laser Doppler perfusion imaging 5 days after injection (Figure 2I). Histological analysis revealed the presence of CD31-positive cells in iECs containing plugs with markedly higher numbers of newly formed vessels compared with control groups (Figure 2J–L). Hence, iECs generated functioning vessels *in vivo*.

Shockwave therapy promotes transdifferentiation in ischaemic myocardium and improves cardiac function

To test whether we could induce transdifferentiation of cardiac fibroblasts to endothelial cells in the ischaemic myocardium, we created a transgenic mouse model of Fsp1-Cre/LacZ mice for lineage tracing (Figure 3A). The left anterior descending coronary artery (LAD) was ligated to induce myocardial infarction of the anterior wall and treated with SWT thereafter. Left ventricular fibrosis was assessed via Masson trichrome staining, and cardiac function was analysed via transthoracic echocardiography 4

weeks after treatment. Indeed, in comparison with untreated controls, SWT reduced the size of fibrotic scar tissue in the LAD occlusion model (Figure 3B and C). Moreover, echocardiography revealed that SWT improved left ventricular ejection fraction and cardiac output and decreased cardiac dilatation (Figure 3D–G) 4 weeks after the experimental myocardial infarction. Induced endothelial cells were identified as cells double positive for LacZ and CD31. Treatment resulted in increased numbers of LacZ/CD31-positive cells in the myocardium indicating induction of transdifferentiation via SWT *in vivo* (Figure 3H and I).

Shockwave therapy induces endothelial-like fibroblast cluster

Next, we performed single-nuclei RNA analysis to further characterize SW effects on the transdifferentiation of fibroblasts *in vivo*. Mice underwent SWT or sham treatment after LAD ligation, and cardiac nuclei were isolated 24 h and 14 days after treatment. Cell type annotation revealed clustering of the cells as expected (Figure 4A; Supplementary material online, Figure S1A). Of interest, pathway analyses of differential expressed genes 14 days after SWT revealed endothelial up-regulation of extracellular vesicle biogenesis (see Supplementary material online, Figure S2A) and activation of TLR, interleukin, and innate immune pathways in fibroblasts (see Supplementary material online, Figure S2B). Compared with controls, SW-treated fibroblasts exhibit up-regulation of angiogenic pathways and TLR signalling, while down-regulating pro-fibrotic pathways such as TGF- β signalling and collagen biosynthesis (see Supplementary material online, Figure S3A–D). Subclustering of the fibroblast population revealed 10 fibroblast clusters (Figure 4B). Intriguingly, Cluster 8 exhibited endothelial cell marker expression including *Cdh5*, *Vwf*, and *Pecam1* (Figure 4C). There was no difference in cell fractions between control and treatment animals; however, we found increased numbers of the fibroblast Subcluster 8 after SWT (Figure 4D; Supplementary material online, Figure S3A). Gene ontology analysis revealed time-dependent changes in this fibroblast cluster post-therapy, with up-regulation of proliferation and endothelial-specific pathways and down-regulation of differentiation and pro-mesenchymal pathways, supporting SWT-induced fibroblast-to-endothelial transdifferentiation *in vivo* (Figure 4E). Trajectory analysis revealed the dynamics of cell fate transitions in the fibroblast clusters and a fibroblast origin of the identified Subcluster 8 (Figure 4E; Supplementary material online, Figure S3B and C).

Shockwave therapy enhances epigenetic plasticity

Epigenetic plasticity is crucial for transdifferentiation and requires inflammatory signalling within the reprogramming cell.⁷ Shockwave therapy and

Figure 2 (Continued)

endothelial cells or fibroblasts after fluorescence-activated cell sorting. red = CD31; blue = DAPI. Scale bar = 20 μ m. (D) Tube formation assay with induced endothelial cells or fibroblasts after fluorescence-activated cell sorting. Scale bar = 50 μ m. (E) Number of nodes per high power field analysed in a tube formation assay in induced endothelial cells or fibroblasts. Data are means \pm SEM. **** P < 0.0001. (F) Number of junctions per high power field analysed in a tube formation assay in induced endothelial cells or fibroblasts. Data are means \pm SEM. **** P < 0.0001. (G) Nitric oxide concentration produced by induced endothelial cells or fibroblasts. Data are means \pm SEM. **** P < 0.0001. (H) Induced endothelial cells, fibroblasts or human umbilical vein endothelial cells were suspended in Matrigel and injected subcutaneously into NSG mice. Blood perfusion of the plug was measured via laser Doppler perfusion imaging (left image). The right image shows the injection sides of the plugs. (I) Blood perfusion of the subcutaneously injected Matrigel plugs containing fibroblasts, induced endothelial cells, or human umbilical vein endothelial cells. Data are means \pm SEM. **** P < 0.0001. (J) Immunofluorescence staining of an induced endothelial cell containing Matrigel plug for CD31. red = CD31; blue = DAPI. Scale bar = 50 μ m. (K) Hematoxylin and eosin staining (H.E.) sections of explanted Matrigel plugs containing fibroblasts, induced endothelial cells, or human umbilical vein endothelial cells analysed for vessels (arrowheads). scale bar = 30 μ m. (L) Number of vessels per high power field in HE stained sections containing fibroblasts, induced endothelial cells, or human umbilical vein endothelial cells. Data are means \pm SEM. * P < 0.05. Statistical comparisons between two groups: Student's *t*-test, multiple groups: one-way analysis of variance with Tukey *post hoc* analysis. HPF, high power field; HUVEC, human umbilical vein endothelial cell; iEC, induced endothelial cell; NO, nitric oxide; VEGF, vascular endothelial growth factor; VEGFR2, VEGF receptor 2.

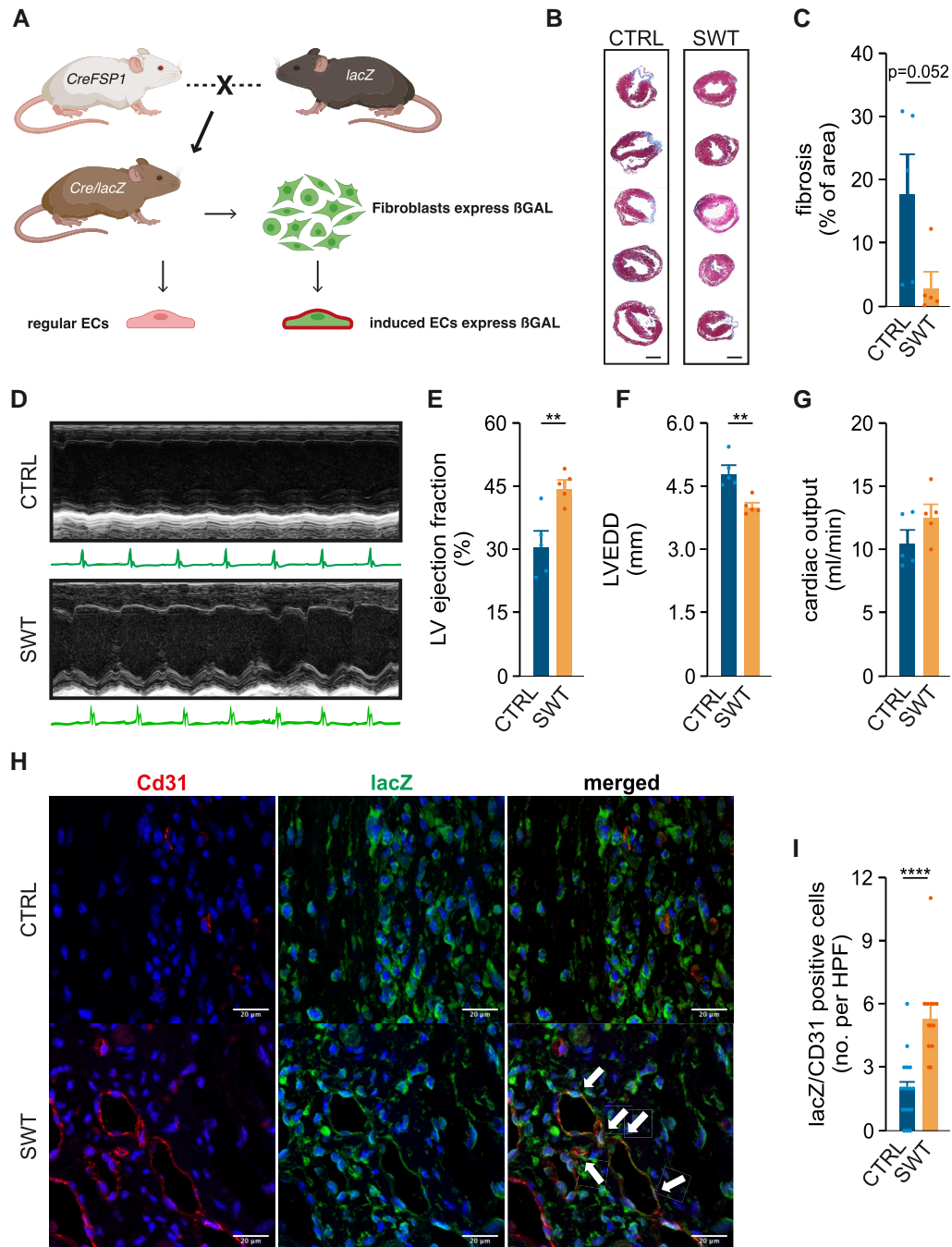


Figure 3 Shockwave therapy induces transdifferentiation in ischaemic myocardium and improves cardiac function. (A) To test whether we could induce transdifferentiation of cardiac fibroblasts within a myocardial scar towards endothelial cells, we created a transgenic mouse model of Fsp1-Cre/LacZ mice and performed a lineage tracing experiment after ligation of the left anterior descending and shockwave therapy. (B) Left ventricular fibrosis assessed via Masson trichrome staining after left anterior descending ligation with (shockwave therapy) or without shockwave therapy (control). Scale bar = 1 mm. (C) Quantification of left ventricular fibrosis after left anterior descending ligation with (shockwave therapy) or without shockwave therapy (control). Data are means \pm SEM. $*P < 0.05$. (D) M-mode images after left anterior descending ligation with (shockwave therapy) or without shockwave therapy (control). (E) Left ventricular ejection fraction after left anterior descending ligation with (shockwave therapy) or without shockwave therapy (control) (%). Data are means \pm SEM. $**P < 0.01$. (F) Left ventricular end-diastolic diameter after left anterior descending ligation with (shockwave therapy) or without shockwave therapy (control) (mm). Data are means \pm SEM. $**P < 0.01$. (G) Cardiac output after left anterior descending ligation with (shockwave therapy) or without shockwave therapy (control) (mL/min). Data are means \pm SEM. (H) Immunofluorescence staining of Fsp1-Cre/LacZ mice after left anterior descending ligation with (shockwave therapy) or without shockwave therapy (control). red = CD31; green = LacZ. blue = DAPI. (I) Number of LacZ/CD31-positive cells after left anterior descending ligation with (shockwave therapy) or without shockwave therapy (control). Data are means \pm SEM. $****P < 0.0001$. Statistical comparisons between two groups: Student's *t*-test, multiple groups: one-way analysis of variance with Tukey *post hoc* analysis. CTRL, control; HPF, high power field; LV, left ventricular; LVEDD, left ventricular end-diastolic diameter; SWT, shockwave therapy.

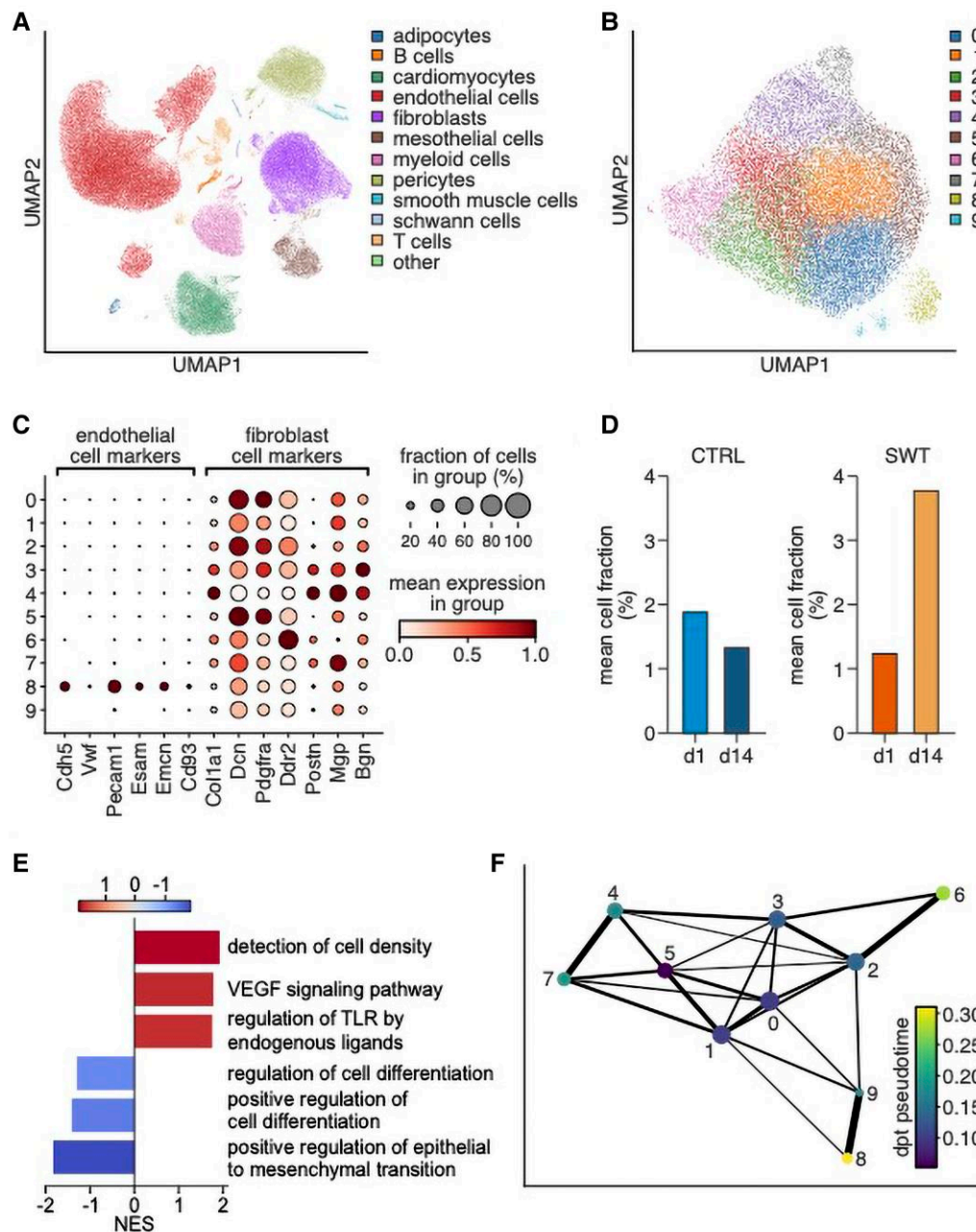


Figure 4 Shockwave-treated hearts show larger endothelial-like fibroblast subcluster after myocardial infarction. (A) Uniform manifold approximation and projection plot showing all sequenced nuclei from all samples from different time points (control Day 1, control Day 14, shockwave (SWT) therapy Day 1, and shockwave therapy Day 14). (B) Uniform manifold approximation and projection plot showing fibroblast subclustering, revealing 10 fibroblast subclusters (Leiden clustering, resolution 0.5). (C) Gene expression of endothelial and fibroblast marker genes in the different fibroblast clusters shown in B. (D) Bar plots showing the relative fibroblast cell fraction of fibroblast Subcluster 8 at different time points. (E) Gene ontology analysis of differentially expressed genes in fibroblast Cluster 8 at 14 days after shockwave therapy vs. control. (F) Partition-based graph abstraction showing cluster dynamics among fibroblast subclusters. Edges represent cluster connectivities; threshold: 0.1). CTRL, control; SWT, shockwave therapy; TLR, Toll-like receptor; UMAP, uniform manifold approximation and projection; VEGF, vascular endothelial growth factor.

TLR3 activation via Poly(I:C) decreased the transcription of the histone modification enzyme histone deacetylase 1 (HDAC1) (see [Supplementary material online, Figure S5A](#)). Moreover, SWT induced up-regulation of PR-domain-containing transcriptional regulator 14 (PRDM14), a key regulator in epigenetic reprogramming via a TLR3-IL-6-STAT3 axis resulting in increased levels of global trimethylation

of H3K4me3 (see [Supplementary material online, Figures S5B–D and S6A–C](#)).^{28,29} This specific histone modification facilitates active gene transcription displaying a crucial step in cellular reprogramming.³⁰ Specific inhibition of this pathway abolished the expression of PRDM14 upon SWT (see [Supplementary material online, Figures S5E and S6B](#)). However, to analyse whether SWT indeed enhances chromatin

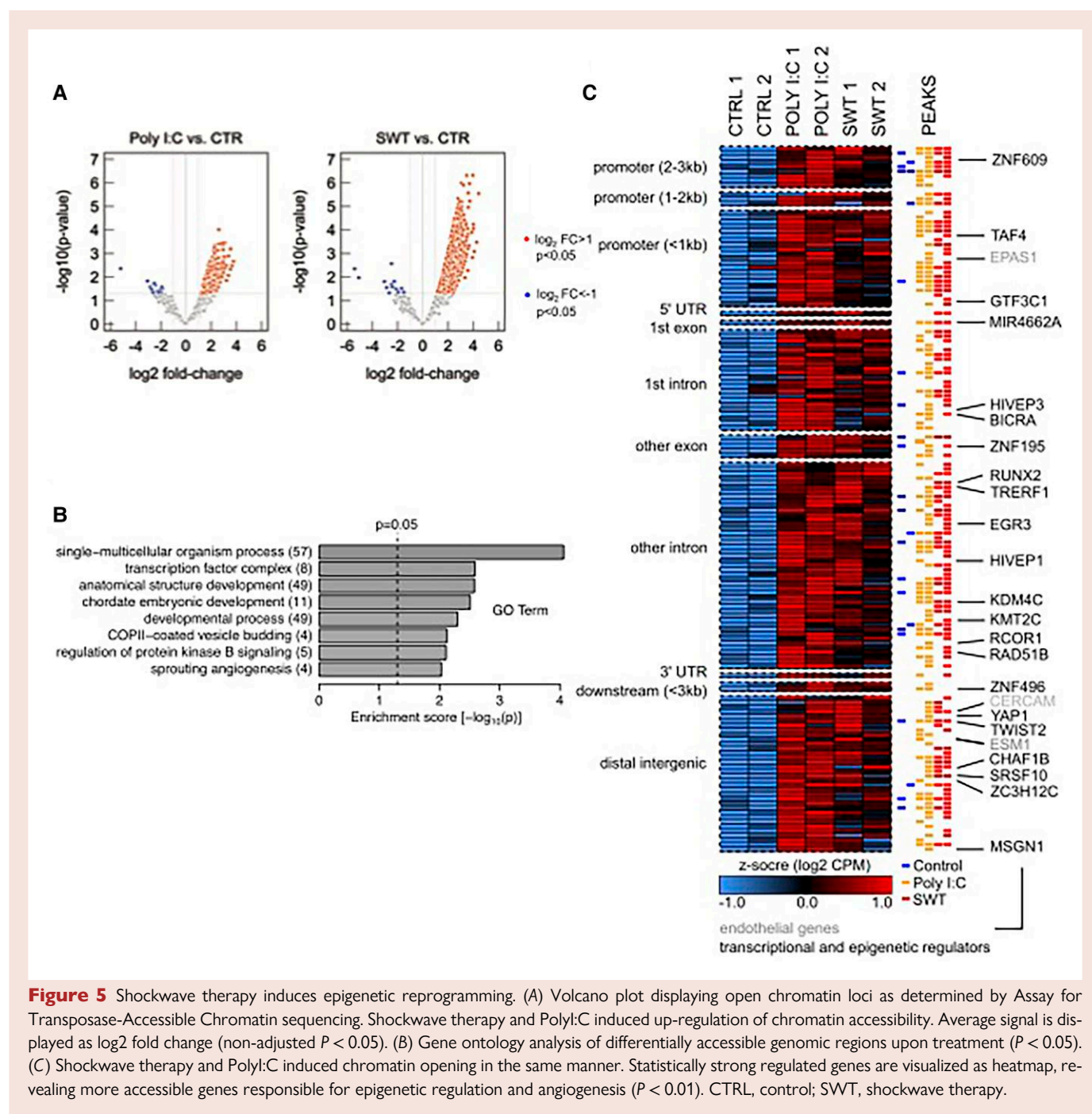


Figure 5 Shockwave therapy induces epigenetic reprogramming. (A) Volcano plot displaying open chromatin loci as determined by Assay for Transposase-Accessible Chromatin sequencing. Shockwave therapy and PolyI:C induced up-regulation of chromatin accessibility. Average signal is displayed as \log_2 fold change (non-adjusted $P < 0.05$). (B) Gene ontology analysis of differentially accessible genomic regions upon treatment ($P < 0.05$). (C) Shockwave therapy and PolyI:C induced chromatin opening in the same manner. Statistically strong regulated genes are visualized as heatmap, revealing more accessible genes responsible for epigenetic regulation and angiogenesis ($P < 0.01$). CTRL, control; SWT, shockwave therapy.

accessibility, we performed global epigenetic profiling of open chromatin via an Assay for Transposase-Accessible Chromatin coupled to high-throughput sequencing (ATAC-Seq) as described previously.²⁰ For this purpose, we treated human cardiac fibroblasts with SWT or Poly(I:C), respectively. Shockwave therapy and Poly(I:C) induced significant changes in chromatin organization, with chromatin being more accessible after both treatments. Notably, both treatments showed effects in the same direction on the chromatin landscape and led exclusively to more accessible gene loci in 1705 genomic regions (Figure 5A). Gene ontology revealed genomic regions with enhanced accessibility responsible for transcription factor complexing, developmental processes, and angiogenesis (Figure 5B; Supplementary material online, Figure S7). We further analysed genomic loci with epigenetic changes of even stronger

statistical significance ($P < 0.01$), which revealed genes involved in epigenetic and transcriptional regulation (Figure 5C). These data indicate that SWT and activation of TLR3 increase DNA accessibility. We compared the genetic landscape with published ATAC data sets and observed no significant group differences (see Supplementary material online, Figure S8). However, this may be attributed to the timing of the analysis, conducted 24 h post-therapy.

Discussion

The salient finding in this study is that mechanical stimulation by SWT facilitates transdifferentiation of cardiac fibroblasts to endothelial cells.

By activating the TLR3 pathway, SWT increases DNA accessibility in cultured fibroblasts, which facilitates their transdifferentiation to iECs under the influence of endothelial growth factors in the medium. These iECs manifested fidelity to an endothelial lineage as shown by immunohistochemical and functional assays *in vitro* and *in vivo*. Notably, in a murine model of myocardial ischaemia, SWT increases capillary density, reduces scar area in the myocardium, and improves ventricular function.

Accumulating data indicates that changes in cell fate require two elements: (i) transcriptional direction, typically provided by transcriptional factors regulating cell lineage, and (ii) DNA accessibility. The most common approach to experimentally altering cell fate is to expose the cells to viral vectors encoding lineage determination factors for the desired cell type. We have shown that viral vectors induce DNA accessibility by activating inflammatory signalling. For example, the Yamanaka approach to generating induced pluripotent stem cells employed a retroviral vector encoding Oct4, Sox2, KLF4, and cMyc (OSKM). We discovered that the Yamanaka factors alone were insufficient for nuclear reprogramming, as cell-permeant peptides of OSKM did not induce pluripotency effectively. However, when an irrelevant retroviral vector was added to the cell permeant factors, appropriate activation of pluripotency genes was observed.⁶ Genetic or pharmacological suppression of TLR3 or RIG1 signalling (which are activated by the viral vector) abrogated nuclear reprogramming to pluripotency.^{6,31} Thus, inflammatory signalling (such as that induced by a viral vector) causes global changes in the expression and activity of epigenetic modifiers to increase DNA accessibility, in a process we term 'transflammation'.⁴

During transflammation, members of the histone acetyltransferase family are up-regulated, whereas members of the histone deacetylase family are down-regulated.⁶ This change in the balance of epigenetic modifiers promotes histone acetylation, which favours an open chromatin state. Furthermore, inducible NO synthesis is up-regulated by inflammatory signalling, translocates to the nucleus, and S-nitrosylates the polycomb repressive complex 1, as well as the NURD complex, removing their suppressive influence on the chromatin.^{32,33} Finally, inflammatory signalling causes a glycolytic shift with mitochondrial export of citrate to the nucleus, providing the substrate for histone acetylation.³⁴ These same inflammatory signalling processes are also required for transdifferentiation of a somatic cell into another lineage.

We showed previously that SWT activates TLR3 via the release of extracellular RNA—possibly packaged in extracellular vesicles²—and induces angiogenesis and vasculogenesis in ischaemic limbs and hearts.³ Of note, cardiac SWT has already been translated into a clinical setting. The CAST-HF trial (Safety and Efficacy of direct Cardiac Shockwave Therapy in patients with ischaemic cardiomyopathy undergoing coronary artery bypass grafting, ClinicalTrials.gov identifier: NCT03859466, cast-trial.com) is a randomized controlled, single-blind monocentric study.¹ Patients with reduced left ventricular ejection fraction ($\leq 40\%$) undergoing coronary artery bypass graft (CABG) surgery were randomized in a 1:1 ratio to receive cardiac SWT (intervention group) or sham treatment (control group). The CAST HF trial showed a significant improvement in left ventricular function, exercise capacity, and quality of life in treated patients.

Our current work shows a molecular mechanism underlying the beneficial effects of SWT. Shockwaves induced TLR3-dependent transdifferentiation of fibroblasts into iECs. The iECs manifested characteristic features of authentic endothelial cells, including the ability to generate NO and to form tube-like structures. In the *in vivo* Matrigel plug assay, inclusion of iECs resulted in greater vascular density within the plug and improved perfusion (in comparison with inclusion of fibroblasts). Whether the identified vessels within the plug were formed by the iECs themselves or due to paracrine effects of the injected iECs remains to be elucidated in future experiments. The extent to which the iECs resemble native endothelial cells at the transcriptional level remains unclear. However, we conducted an extensive characterization of the iECs, incorporating analyses of gene expression, protein expression, and functional properties. These assessments unequivocally

demonstrated the angiogenic potential and functional equivalence of iECs to conventional endothelial cells. Based on our data, iECs are best characterized as endothelial-like cells. However, the distinction from true endothelial cells is likely of limited relevance given their demonstrated functional properties.

To confirm that SWT induces transdifferentiation *in vivo*, we performed a lineage tracing experiment. For this purpose, we used a LAD ligation model in transgenic Fsp1-Cre/LacZ mice. The ideal marker for cardiac fibroblasts remains controversial.^{35,36} Nevertheless, we performed a lineage tracing experiment using Fsp1-Cre/LacZ mice.^{37,38} In this model, we found higher numbers of iECs after SWT of the ischaemic myocardium. These findings were associated with a decreased area of myocardial fibrosis and improved left ventricular function. Hence, we could show for the first time the induction of cellular reprogramming *in vivo* with a therapeutic method already in clinical use. While *in vitro* transdifferentiation is facilitated by growth factors supplied by the induction medium, transcriptional direction *in vivo* is provided by the pro-angiogenic microenvironment, driven by hypoxia, inflammation, and the release of growth factors and cytokines from ischaemic tissue.³⁹ Shockwave therapy further contributes by releasing growth factors stored in the extracellular matrix and promoting the release of angiogenic extracellular vesicles, with endothelial cells likely being the primary contributors, although the precise cellular source remains uncertain.^{25,40} However, the higher *in vivo* transdifferentiation ($\sim 4\%$ vs. 1% *in vitro*) reflects the supportive microenvironment, suggesting SW-induced transdifferentiation complements VEGF-driven angiogenesis. While a reduction in pro-fibrotic pathways was observed, no antiproliferative effects were detected in fibroblasts. Shockwave therapy predominantly reduces infarct size and fibrosis by enhancing capillary density and oxygenation in the border zone, improving perfusion and myocardial salvage. Still, an additional analysis using an alternative lineage tracing model may be necessary to further validate the effectiveness of *in vivo* transdifferentiation.

The mouse model used has some limitations because it mainly represents chronic ischaemic heart disease. In the CAST-HF trial, SWT was given after CABG, once blood flow to the heart was restored, which may have boosted its effects. While patients have conditions like atherosclerosis and microvascular dysfunction that are not present in mice, the chronic ischaemia model after LAD ligation is still a valuable model to investigate angiogenesis in ischaemic myocardium.

Upon TLR3 activation, NF- κ B-dependent transcription of IL-6 mediates the inflammatory cascade resulting in cellular reprogramming.^{6,41,42} We observed that SWT induces histone modifications associated with open chromatin. The ATAC-seq studies revealed enhanced chromatin accessibility upon TLR3 activation by SWT. Hence, SWT induces chromatin remodelling and, thus, promotes cellular plasticity.

Altogether, we provide evidence for the induction of transdifferentiation in ischaemic myocardium via SWT. Shockwave therapy could become a feasible technology to promote therapeutic transdifferentiation providing a novel approach to address the global burden of ischaemic heart failure.

Lead author biography



Michael Graber is an Austrian cardiac surgery resident at the Medical University of Innsbruck, Austria. His academic background includes a PhD in Molecular Cell Biology and a completed postdoctoral fellowship at the Houston Methodist Research Institute in the USA. His research focus is mainly on translational research with particular interest in myocardial regeneration and valvular heart disease.

Data availability

All high-throughput data are available via GEO. The data sets generated and/or analysed during this study are available from the corresponding author on reasonable request.

Supplementary material

Supplementary material is available at *European Heart Journal Open* online.

Funding

This work was supported by an AUVA unrestricted research grant to J. Holfeld and C.G.-T. and grants to J.P.C. from the National Heart, Lung and Blood Institute (1R01HL148338 and 1R01HL133254). F.E. is supported by a PhD fellowship of the Austrian Academy of Sciences.

Conflict of interest: J. Holfeld, M. Grimm, and J.P.C. are shareholders of Heart Regeneration Technologies GmbH, an Innsbruck Medical University spin-off aiming to promote cardiac shockwave therapy (www.heart-regeneration.com). J.P.C. is an inventor on patents held by Stanford University on the use of innate immune signalling for modulation of cell fate by mRNA therapeutics. All other authors have nothing to disclose.

References

- Holfeld J, Nägele F, Polzl L, Engler C, Graber M, Hirsch J, Schmidt S, Mayr A, Troger F, Pamminger M, Theurl M, Schreinlechner M, Sappeler N, Ruttman-Ulmer E, Schaden W, Cooke JP, Ulmer H, Bauer A, Gollmann-Tepeköylü C, Grimm M. Cardiac shockwave therapy in addition to coronary bypass surgery improves myocardial function in ischaemic heart failure: the CAST-HF trial. *Eur Heart J* 2024;**45**:2634–2643.
- Gollmann-Tepeköylü C, Polzl L, Graber M, Hirsch J, Nägele F, Lobenstein D, Hess MW, Blumer MJ, Kirchmair E, Zipperle J, Hromada C, Mühleder S, Hackl H, Hermann M, Al Khamisi H, Förster M, Lichtenauer M, Mittermayr R, Paulus P, Fritsch H, Bonaros N, Kirchmair R, Sluijter JPG, Davidson S, Grimm M, Holfeld J. miR-19a-3p containing exosomes improve function of ischemic myocardium upon shock wave therapy. *Cardiovasc Res* 2020;**116**:1226–1236.
- Holfeld J, Tepeköylü C, Reissig C, Lobenstein D, Scheller B, Kirchmair E, Kozaryn R, Albrecht-Schöer K, Krapf C, Zins K, Urbschat A, Zacharowski K, Grimm M, Kirchmair R, Paulus P. Toll-like receptor 3 signalling mediates angiogenic response upon shock wave treatment of ischaemic muscle. *Cardiovasc Res* 2016;**109**:331–343.
- Cooke JP. Therapeutic transdifferentiation: a novel approach for vascular disease. *Circ Res* 2013;**112**:748–750.
- Pang ZP, Yang N, Vierbuchen T, Ostermeier A, Fuentes DR, Yang TQ, Citri A, Sebastiano V, Marro S, Südhof TC, Wernig M. Induction of human neuronal cells by defined transcription factors. *Nature* 2011;**476**:220–223.
- Lee J, Sayed N, Hunter A, Au KF, Wong WH, Mocarski ES, Pera RR, Yakubov E, Cooke JP. Activation of innate immunity is required for efficient nuclear reprogramming. *Cell* 2012;**151**:547–558.
- Sayed N, Wong WT, Ospino F, Meng S, Lee J, Jha A, Dexheimer P, Aronow BJ, Cooke JP. Transdifferentiation of human fibroblasts to endothelial cells: role of innate immunity. *Circulation* 2015;**131**:300–309.
- Ginsberg M, James D, Ding BS, Nolan D, Geng F, Butler JM, Schachterle W, Pulijal VR, Mathew S, Chasen ST, Xiang J, Rosenwaks Z, Shido K, Elemento O, Rabbany SY, Rafii S. Efficient direct reprogramming of mature amniotic cells into endothelial cells by ETS factors and TGF β suppression. *Cell* 2012;**151**:559–575.
- Gollmann-Tepeköylü C, Graber M, Polzl L, Nägele F, Moling R, Esser H, Summerer B, Mellitzer V, Ebner S, Hirsch J, Schäfer G, Hackl H, Cardini B, Oberhuber R, Primavesi F, Öfner D, Bonaros N, Troppmair J, Grimm M, Schneeberger S, Holfeld J, Resch T. Toll-like receptor 3 mediates ischaemia/reperfusion injury after cardiac transplantation. *Eur J Cardiothorac Surg* 2020;**57**:826–835.
- Holfeld J, Tepeköylü C, Kozaryn R, Mathes W, Grimm M, Paulus P. Shock wave application to cell cultures. *J Vis Exp* 2014;51076. <https://doi.org/10.3791/51076>
- DeCicco-Skinner KL, Henry GH, Cattaillon C, Tabib T, Gwilliam JC, Watson NJ, Bullwinkle EM, Falkenburg L, O'Neill RC, Morin A. Endothelial cell tube formation assay for the in vitro study of angiogenesis. *J Vis Exp* 2014;e51312. <https://doi.org/10.3791/51312>
- Kastana P, Zahra FT, Ntenekou D, Katraki-Pavlou S, Beis D, Lionakis MS, Mikelis CM, Papadimitriou E. Matrigel plug assay for in vivo evaluation of angiogenesis. *Methods in Molecular Biology* 2019;**1952**:219–232.
- Ewels PA, Peltzer A, Fillinger S, Patel H, Alneberg J, Wilm A, Garcia MU, Di Tommaso P, Nahnsen S. The nf-core framework for community-curated bioinformatics pipelines. *Nat Biotechnol* 2020;**38**:276–278.
- Wolf FA, Angerer P, Theis FJ. SCANPY: large-scale single-cell gene expression data analysis. *Genome Biol* 2018;**19**:15.
- Sheng C, Lopes R, Li G, Schuierer S, Waldt A, Cuttat R, Dimitrieva S, Kauffmann A, Durand E, Galli GG, Roma G, de Weck A. Probabilistic machine learning ensures accurate ambient denoising in droplet-based single-cell omics. *bioRxiv*, <https://doi.org/10.1101/2022.01.14.476312>, 24 March 2022, preprint: not peer reviewed.
- Gayoso A, Lopez R, Xing G, Boyeau P, Valiollah Pour Amiri V, Hong J, Wu K, Jayasuriya M, Mehlman E, Langevin M, Liu Y, Samaran J, Misrahi G, Nazaret A, Clivio O, Xu C, Ashuach T, Gabitto M, Lotfollahi M, Svensson V, da Veiga Beltrame E, Kleshcheynikov V, Talavera-López C, Pachter L, Theis FJ, Streets A, Jordan MI, Regier J, Yosef N. A Python library for probabilistic analysis of single-cell omics data. *Nat Biotechnol* 2022;**40**:163–166.
- Bernstein NJ, Fong NL, Lam I, Roy MA, Hendrickson DG, Kelley DR. Solo: doublet identification in single-cell RNA-seq via semi-supervised deep learning. *Cell Syst* 2020;**11**:95–101.e5.
- Skelly DA, Squiers GT, McLellan MA, Bolisetty MT, Robson P, Rosenthal NA, Pinto AR. Single-cell transcriptional profiling reveals cellular diversity and intercommunication in the mouse heart. *Cell Rep* 2018;**22**:600–610.
- Tombor LS, John D, Glaser SF, Luxán G, Forte E, Furtado M, Rosenthal N, Baumgarten N, Schulz MH, Wittig J, Rogg E-M, Manavski Y, Fischer A, Muhly-Reinholz M, Klee K, Looso M, Selignow C, Acker T, Bibli S-I, Fleming I, Patrick R, Harvey RP, Abplanalp WT, Dimmeler S. Single cell sequencing reveals endothelial plasticity with transient mesenchymal activation after myocardial infarction. *Nat Commun* 2021;**12**:681.
- Molenaar B, Timmer LT, Droog M, Perini I, Versteeg D, Kooijman L, Monshouwer-Kloots J, de Ruiter H, Gladka MM, van Rooij E. Single-cell transcriptomics following ischemic injury identifies a role for B2M in cardiac repair. *Commun Biol* 2021;**4**:146.
- Haghverdi L, Büttner M, Wolf FA, Büttner F, Theis FJ. Diffusion pseudotime robustly reconstructs lineage branching. *Nat Methods* 2016;**13**:845–848.
- Wolf FA, Hamey FK, Plass M, Solana J, Dahlin JS, Göttgens B, Rajewsky N, Simon L, Theis FJ. PAGA: graph abstraction reconciles clustering with trajectory inference through a topology preserving map of single cells. *Genome Biol* 2019;**20**:59.
- Reske JJ, Wilson MR, Chandler RL. ATAC-seq normalization method can significantly affect differential accessibility analysis and interpretation. *Epigenetics Chromatin* 2020;**13**:22.
- Albus U, Albus U. Guide for the care and use of laboratory animals (8th edn). *Lab Anim* 2012;**46**:267–268.
- Gollmann-Tepeköylü C, Lobenstein D, Theurl M, Primessnig U, Lener D, Kirchmair E, Mathes W, Graber M, Polzl L, An A, Koziel K, Pechriggl E, Voelkl J, Paulus P, Schaden W, Grimm M, Kirchmair R, Holfeld J. Shock wave therapy improves cardiac function in a model of chronic ischemic heart failure: evidence for a mechanism involving VEGF signaling and the extracellular matrix. *J Am Heart Assoc* 2018;**7**:e010025.
- Respress JL, Wehrens XHT. Transthoracic echocardiography in mice. *J Vis Exp* 2010:1738. <https://doi.org/10.3791/1738>
- Valentin J, Frobert A, Ajabert G, Cook S, Giraud M-N. Histological quantification of chronic myocardial infarct in rats. *J Vis Exp* 2016;54914. <https://doi.org/10.3791/54914>
- Nakaki F, Saitou M. PRDM14: a unique regulator for pluripotency and epigenetic reprogramming. *Trends Biochem Sci* 2014;**39**:289–298.
- Chen H, Aksoy I, Gonnot F, Osteil P, Aubry M, Hamela C, Rognard C, Hochard A, Voisin S, Fontaine E, Mure M, Afanassieff M, Cleroux E, Guibert S, Chen J, Vallot C, Acloque H, Genthon C, Donnadiou C, De Vos J, Sanlaville D, Guérin J-F, Weber M, Stanton LW, Rougeulle C, Pain B, Bourillot P-Y, Savatier P. Reinforcement of STAT3 activity reprograms human embryonic stem cells to naive-like pluripotency. *Nat Commun* 2015;**6**:7095.
- Santos-Rosa H, Schneider R, Bannister AJ, Sheriff J, Bernstein BE, Emre NCT, Schreiber SL, Mellor J, Kouzarides T. Active genes are tri-methylated at K4 of histone H3. *Nature* 2002;**419**:407–411.
- Sayed N, Ospino F, Himmati F, Lee J, Chanda P, Mocarski ES, Cooke JP. Retinoic acid inducible gene 1 protein (RIG1)-like receptor pathway is required for efficient nuclear reprogramming. *Stem Cells* 2017;**35**:1197–1207.
- Meng S, Zhou G, Gu Q, Chanda PK, Ospino F, Cooke JP. Transdifferentiation requires iNOS activation: role of RING1A S-nitrosylation. *Circ Res* 2016;**119**:e129–e138.
- Chanda PK, Meng S, Lee J, Leung HE, Chen K, Cooke JP. Nuclear S-nitrosylation defines an optimal zone for inducing pluripotency. *Circulation* 2019;**140**:1081–1099.
- Lai L, Reineke E, Hamilton DJ, Cooke JP. Glycolytic switch is required for transdifferentiation to endothelial lineage. *Circulation* 2019;**139**:119–133.
- Fu X, Liu Q, Li C, Li Y, Wang L. Cardiac fibrosis and cardiac fibroblast lineage-tracing: recent advances. *Front Physiol* 2020;**11**:416.
- Kalluri R, Zeisberg M. Fibroblasts in cancer. *Nat Rev Cancer* 2006;**6**:582–598.

37. Qian L, Huang Y, Spencer CI, Foley A, Vedantham V, Liu L, Conway SJ, Fu J-D, Srivastava D. In vivo reprogramming of murine cardiac fibroblasts into induced cardiomyocytes. *Nature* 2012;**485**:593–598.
38. Song K, Nam Y-J, Luo X, Qi X, Tan W, Huang GN, Acharya A, Smith CL, Tallquist MD, Neilson EG, Hill JA, Bassel-Duby R, Olson EN. Heart repair by reprogramming non-myocytes with cardiac transcription factors. *Nature* 2012;**485**:599–604.
39. Zhao Y, Xiong W, Li C, Zhao R, Lu H, Song S, Zhou Y, Hu Y, Shi B, Ge J. Hypoxia-induced signaling in the cardiovascular system: pathogenesis and therapeutic targets. *Signal Transduct Target Ther* 2023;**8**:431.
40. Holfeld J, Tepekoylu C, Blunder S, Lobenwein D, Kirchmair E, Dietl M, Kozaryn R, Lener D, Theurl M, Paulus P, Kirchmair R, Grimm M. Low energy shock wave therapy induces angiogenesis in acute hind-limb ischemia via VEGF receptor 2 phosphorylation. *PLoS One* 2014;**9**:e103982.
41. Meng S, Lv J, Chanda PK, Owusu I, Chen K, Cooke JP. Reservoir of fibroblasts promotes recovery from limb ischemia. *Circulation* 2020;**142**:1647–1662.
42. Iliopoulos D, Hirsch HA, Struhl K. An epigenetic switch involving NF- κ B, Lin28, Let-7 MicroRNA, and IL6 links inflammation to cell transformation. *Cell* 2009;**139**:693–706.